Supplementary Information

Supplementary Methods

Cell culture

The human adenocarcinoma alveolar epithelial A549 cell line (CCL-185), murine Lewis lung carcinoma (LLC-1) cell line (CRL-1642), and murine B16F1 melanoma cell line (CRL-6323) were obtained from ATCC. The A549 cells were cultured in DMEM/F12 medium supplemented with 10% FBS (v/v), 100 IU mL^{-1} penicillin, 100 μg mL^{-1} streptomycin, and 2 mM Gluta-max (Gibco) in a 95% humidified atmosphere containing 5% CO_2 at 37 °C. The LLC-1 cell line was cultured in DMEM, while the B16F1 cell line was cultured in DMEM/F12 medium supplemented with 10% FBS (v/v), 100 IU mL^{-1} penicillin, and 100 μg mL^{-1} streptomycin in a 95% humidified atmosphere containing 5% CO_2 at 37 °C. Passages 2–10 were used in this study.

In vivo CT imaging

To perform CT imaging, anesthetized mice with B16F1 tumors were injected with Y-BTC (100 mg mL^{-1}, 88 μL per 200 μL of tumor) in saline. Whole-body CT imaging was performed on a U-SPECT-II/CT scanner (MILabs, Utrecht, Netherlands) using a standard protocol with 45 kV and 500 μA. The CT imaging parameters were as follows: pixel size, 80 μm; field of view, 82 mm length × 41 mm diameter; rotation, 360°; step, 0.72°. The CT scans were collected and reconstructed using the manufacturer's software. PMOD 3.4 (PMOD Technologies Ltd., Switzerland) was used for 3D reconstruction and imaging.

Dosimetry for treatments

To calculate the absorbed radiation doses to tumors and cells from ^{90}Y-containing formulations, we used the medical internal radiation dose (MIRD) method. In the MIRD schema, the absorbed dose $D_{\bar{r}_T}(t)$ to target tissue $\bar{r}_T$ over a dose integration period t was calculated as follows:

$$D_{\bar{r}_T}(t) = \bar{A}_{\bar{r}_S}(t) \times S(\bar{r}_T \leftarrow \bar{r}_S, t),$$

where $\bar{A}_{\bar{r}_S}(t)$ represents the time-integrated activity (i.e., the total number of nuclear transformations) in the source tissue $\bar{r}_S$, and $S(\bar{r}_T \leftarrow \bar{r}_S, t)$ denotes the mean absorbed dose rate to the target region $\bar{r}_T$, at time t after administration per unit activity in the source region $\bar{r}_S$. For injected tumors, the source and target regions are the same. The S value is specifically determined for ^{90}Y emissions based on the geometry and density of the tumor:

$$S(\bar{r}_T \leftarrow \bar{r}_S, t) = \frac{\sum_i E_i \cdot n_i \cdot \varphi(\bar{r}_T \leftarrow \bar{r}_S; E_i, t)}{m_{\bar{r}_T}(t)},$$

where $m_{\bar{r}_T}(t)$ represents the time-dependent mass of the target tissue, n is a number of particles (or photons) with energy E emitted per nuclear transformation in the radionuclide decay scheme, $\varphi(\bar{r}_T \leftarrow \bar{r}_S; E_i, t)$ is the absorbed fraction of energy E, which is emitted at time t from the source region $\bar{r}_S$ and is absorbed in the target volume $\bar{r}_T$. For our calculations, it was assumed that $\varphi(\bar{r}_T \leftarrow \bar{r}_S; E_i, t) = 1$.

Histological analysis

Tissues from the bone marrow, heart, lung, and liver were collected from two mice in the control group (on day 5) and two mice in the ^{90}Y,Y-BTC microparticle-treated group (on day 11). The excised samples were placed in a 10% formalin solution for fixation. The tissues were then dehydrated, embedded in paraffin, cut into 5–6 μm-thick sections, and stained with hematoxylin and eosin. Analysis was performed using an Olympus CX41 microscope (Olympus Co., Tokyo, Japan), equipped with a UPlanApo 20×/NA 0.70 objective lens.

Supplementary Figures

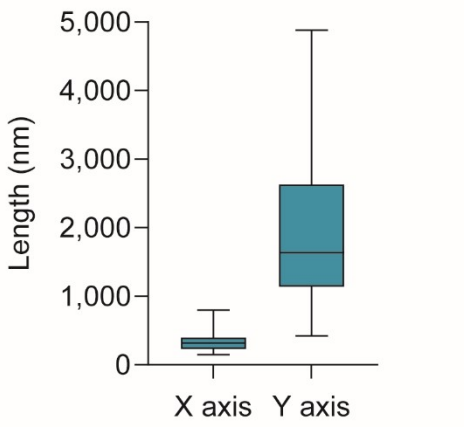

Figure S1. Size distribution of Y-BTC miroparticles for X and Y axis determined by quantitative analysis of SEM images. Over 30 particles were measured. Approximate aspect ratio is 1:6. The data are expressed as the mean ± SD.

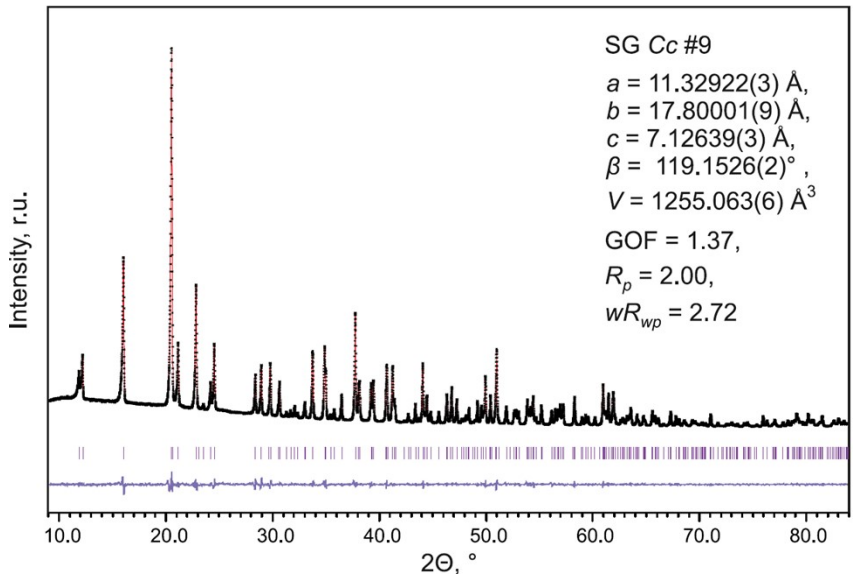

Figure S2. Powder X-ray diffraction pattern of experimental Y-BTC particles (Co-$K_{\alpha 1}$ radiation).

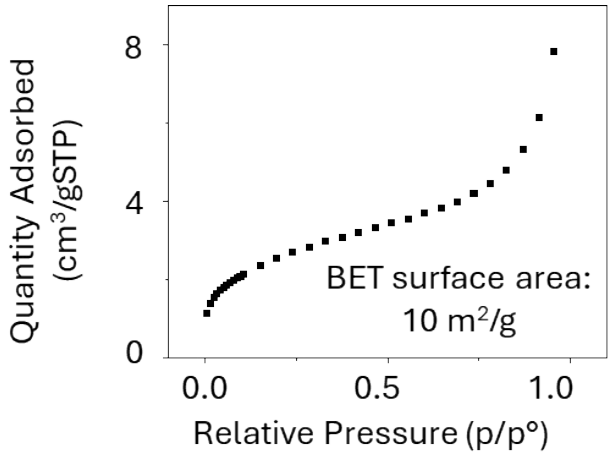

Figure S3. Nitrogen adsorption analysis of Y-BTC.

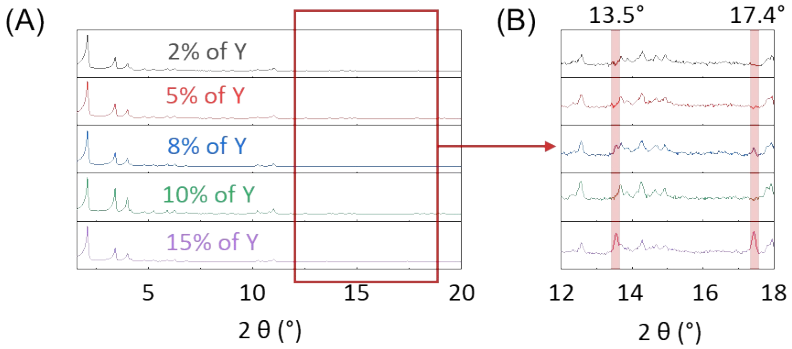

Figure S4. (A) PXRD pattern of MIL-100(Fe,Y) with n(Y)/[n(Y)+n(Fe)] ratios ranging from 2% to 15%. (B) Magnified PXRD pattern focusing on the range from 12 to 18°, highlighting the peaks at 13.5° and 17.4°, which correspond to the presence of $Y(BTC)(H_2O)_6$.

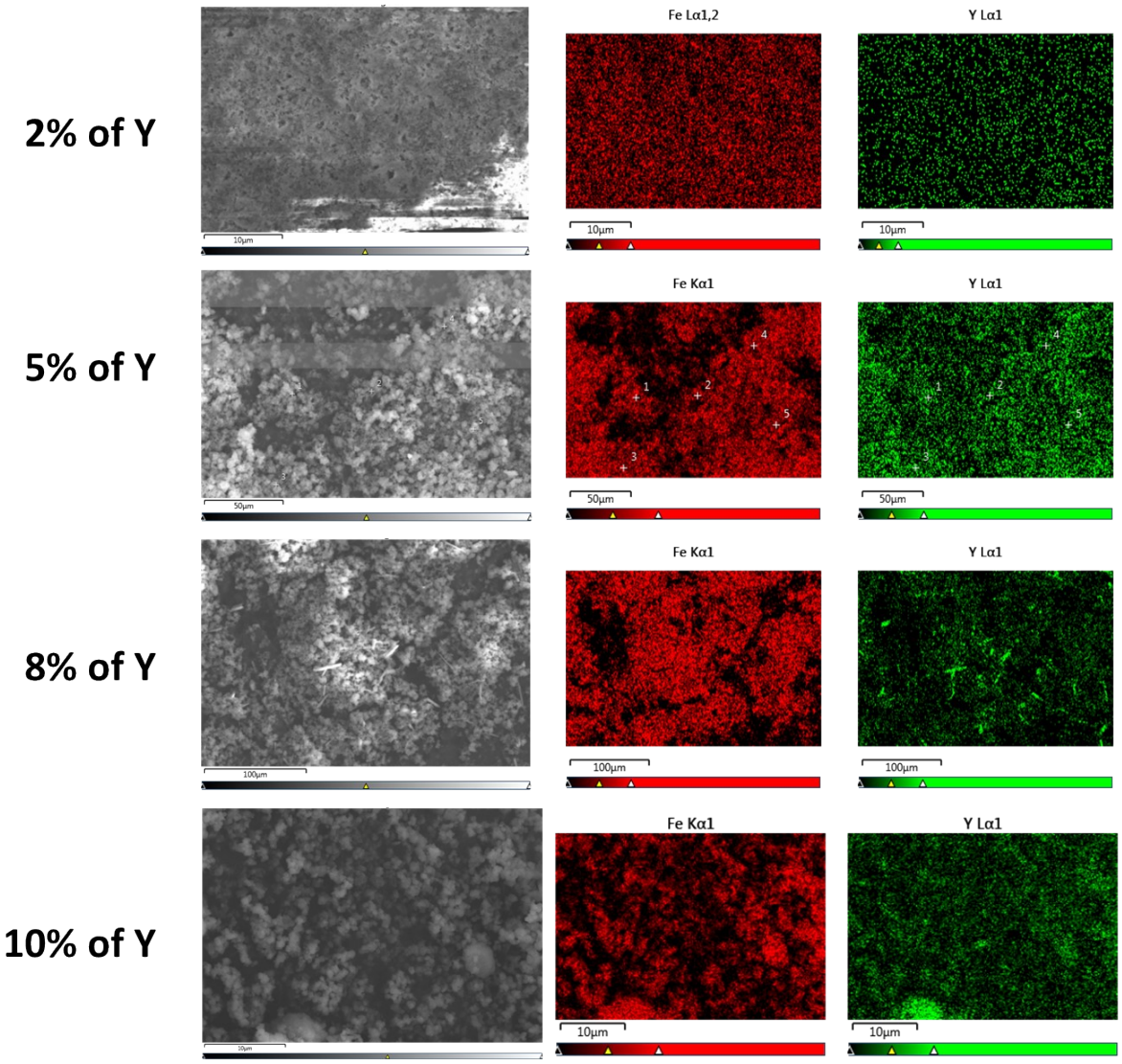

Figure S5. SEM EDX map of MIL-100(Fe,Y) particles with 2, 5, 8, and 10% of doped Y. The scale bar is 10 μm.

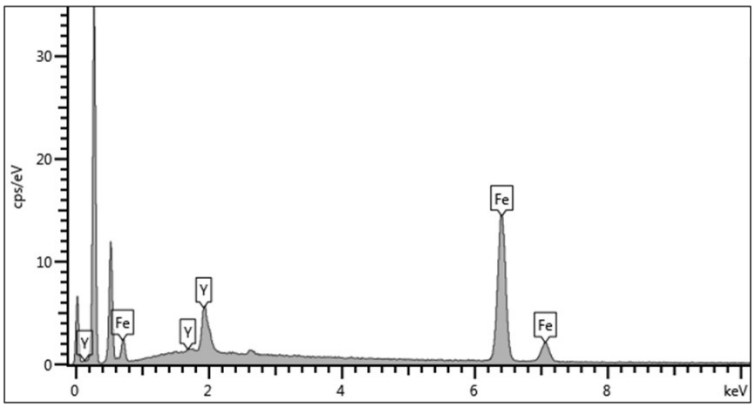

Figure S6. SEM-EDX spectrum of MIL-100(Fe, Y) with n(Y)/[n(Y)+n(Fe)] ratios at 10% of doped Y.

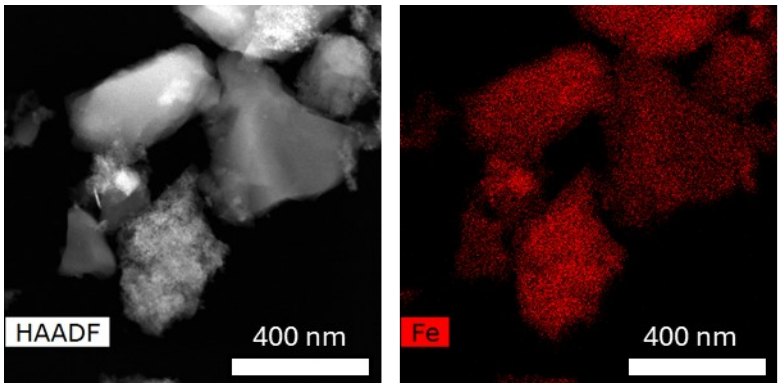

Figure S7. STEM-HAADF EDX map of MIL-100(Fe) particles.

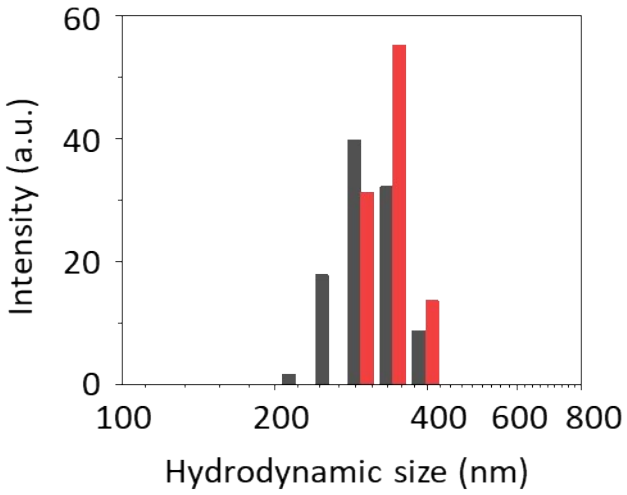

Figure S8. Hydrodynamic size of MIL-100(Fe) (dark grey) and MIL-100(Fe,Y) (red) in PBS (pH=7.4).

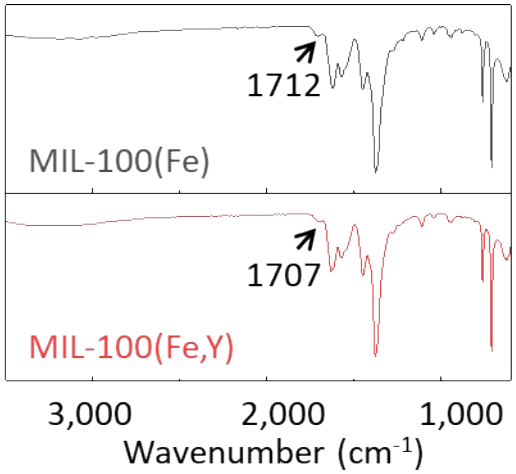

Figure S9. FT-IR spectra of MIL-100(Fe) and MIL-100(Fe,Y).

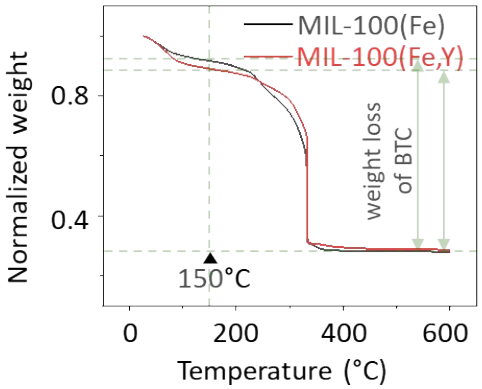

Figure S10. TGA curve of MIL-100(Fe) and MIL-100(Fe,Y), the mass of MIL-100(Fe) and MIL-100(Fe,Y) particles at 25 °C was normalized to "1".

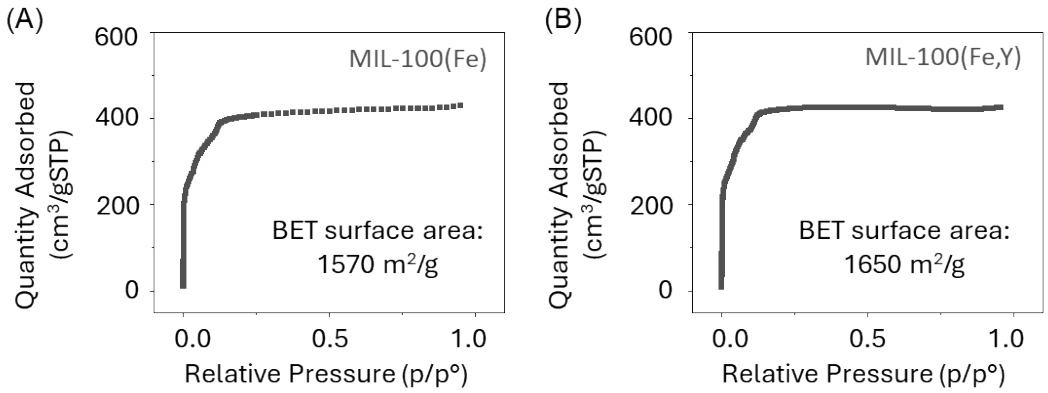

Figure S11. Nitrogen adsorption analysis of (A) MIL-100(Fe) and (B) MIL-100(Fe,Y).

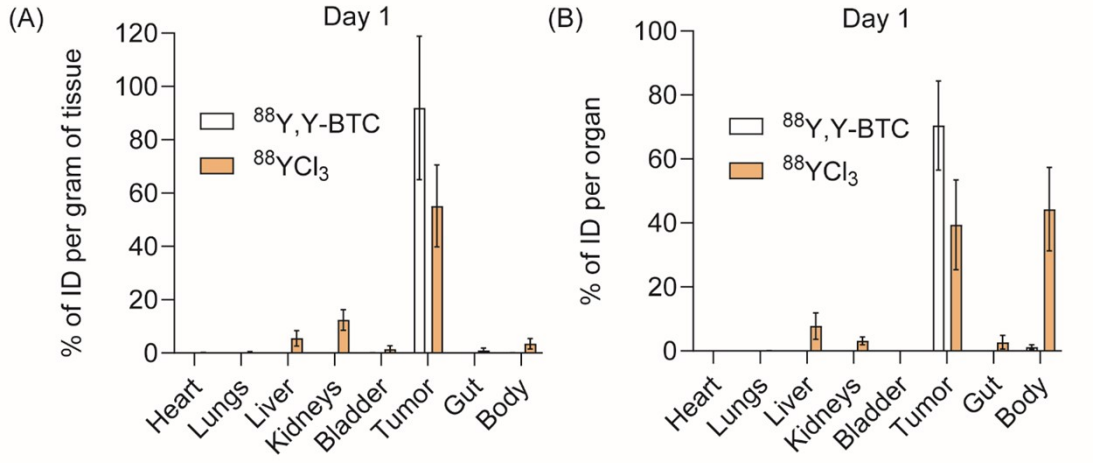

Figure S12. Yttrium-88 retention at tumor site after intratumoral injection of ^{88}Y,Y-BTC-doped MOFs or $^{88}YCl_3$. (A) Radioactivity measurements in different tissues on day 1 after treatment with ^{88}Y,Y-BTC particles compared to $^{88}YCl_3$ shown as the percentage of injected dose (ID) per gram of tissue and (B) per organ. The data are expressed as the mean ± SD (n = 3).

Supplementary Tables

Table S1. Comparison of Y molar ratios during synthesis and in resulting samples measured by SEM-EDX.

n(Y)/[n(Y)+n(Fe)] (%)	
during synthesis	**measured by SEM-EDX ± error**
2	2.39 ± 0.59
5	7.66 ± 1.22
8	10.50 ± 1.83
10	12.73 ± 1.58

Table S2. Intensity mean size and mean zeta potential of MIL-100(Fe) and MIL-100(Fe,Y) particles.

Samples	Intensity mean size (nm)	PdI	Zeta potential (mV)
MIL-100(Fe)	344.5 ± 27.3	0.7	-23.0 ± 1.8
MIL-100(Fe,Y)	352.5 ± 91.5	0.7	-24.3 ± 1.3